Green Chemistry

Mechanistic Studies of Milled and Kraft Lignin Oxidation by Radical Species

Journal:	*Green Chemistry*
Manuscript ID	GC-ART-12-2019-004162
Article Type:	Paper
Date Submitted by the Author:	05-Dec-2019
Complete List of Authors:	Davaritouchaee, Maryam; Washington State University, Chemical Engineering Hiscox, Bill; Washington State University, Department of Chemistry Terrell, Evan; Washington State University, Department of Biological Systems Engineering Mancini, Rock; Washington State University, Chemistry Chen, Shulin; Washington State University, Biological and Agricultural engineering

Mechanistic Studies of Milled and Kraft Lignin Oxidation by Radical Species

Maryam Davaritouchaee[1], William C. Hiscox[2], Evan Terrell[3], Rock J. Mancini[1,4], Shulin Chen[3*]

[1] The Gene & Linda Voiland School of Chemical Engineering and Bioengineering, Washington State University, Pullman, WA, USA

[2] Center for NMR Spectroscopy, Department of Chemistry, Washington State University, Pullman, WA, USA

[3] Department of Biological Systems Engineering, Washington State University, Pullman, WA, USA

[4] Department of Chemistry, Washington State University, Pullman, WA, USA

Corresponding author E-mail address: Chens@wsu.edu

Abstract

Accomplishing selective lignin degradation in a controlled manner by breaking C–O and C–C bonds is of great scientific interest although technically challenging. The structural modification of two different types of lignin (milled and Kraft) subjected to four sources of radicals (superoxide, sulfate, hydroperoxide, and hydroxyl radicals) was studied for achieving such a purpose. The treatments with superoxide and hydroperoxide radicals increased the number of alkyl group substituents and H lignin subunits while sulfate and hydroxyl radicals preferentially reacted via lignin side-chain oxidation. The efficiency of lignin cleavage, based on reduced molecular weight (*Mw*)

as a result of oxidation, was found to be generally in the order of superoxide, sulfate, hydroperoxide, and hydroxyl radicals initiators. Characterizing the radical degradation products revealed that C–C cleavage of phenyl coumarin and resinol substructures was the predominant mechanism in superoxide radical oxidation, whereas β–O–4 cleavage and side-chain oxidation were the main pathways in the sulfate radical treatment. Moreover, superoxide and hydroperoxide radical treatments shifted lignin thermolysis peaks to lower temperature. However, in sulfate and hydroxyl radicals methods, due to condensation reactions, some stable lignin-like polymers were generated which required higher degradation temperatures. Collectively, the results demonstrated the different ways of lignin structure alteration by different radical oxidation sources and highlighted the reaction features of each radical tested.

Keywords: Radical species, Lignin degradation, Selective oxidation, Linkages cleavage, Reactivity trends.

Introduction

Unlocking plant cell walls by pretreatment to separate their components such as polysaccharides and lignin has been long practiced.[1] However, targeted modification of lignin during or after the separation remains a technical challenge. It is of great interest in many applications such as cellulosic biofuels to separate lignin from whole biomass to not only liberate carbohydrates to be used in the downstream conversion but also to break purposely lignin to small molecule as co-products. Addressing such a needs depends on the in-depth understanding of the cleavage of the specific bonds within the reaction systems.

Lignin is a polymeric molecule made up of aromatic phenolic and methoxy-phenolic

units containing propanoid side chains (coumaryl alcohol or H unit, coniferyl alcohol or G unit, and sinapyl alcohol or S unit).[2, 3] Lignin sub-units are linked through various non-uniform C–C and C–O–C bonds such as β-O-4', β-5', β-β', β-1, 5-5, and α-O-4 to form the overall random 3-D polymeric structure.[4] Lignin, as a highly functionalized natural polymer derived from lignocellulosic biomass, is a by-product of pulp and paper and biofuel industries. This biopolymer, amounting up to 40 million tons a year from pulping processes alone, is considered as a potentially valuable source of renewable feedstocks for producing biochemical or bioproducts, especially aromatic hydrocarbons.[5] Despite this potential, commercializing these high value applications has been very limited. Although numerous attempts have been made to valorize lignin, degrading the complex structure of lignin to specific small-molecules remains as a major challenge.[6] Consequently, the majority of these by-product polymers is being burned as a low-value type of energy.[6] Ideally, controlled cleavage of C–C and C–O–C bonds in lignin would be beneficial because it could lead to more selective depolymerization of the polymer to value-added small-molecules. This specific bond-breaking strategy offers an avenue for producing a series of monomeric compounds with numerous potential applications in pharmaceuticals, nutraceuticals, polymers, additives, and fine chemicals.[7, 8]

Lignin degradation studies have usually been conducted with chemically defined lignin model compounds.[7] These studies while providing a more accessible platform for monitoring degradation and identifying derivative products, do not take into account complexities arising from the complete structure of lignin and secondary conditions, such as polarity, counterions, impurities, and the abundance of functional groups in the natural polymer. In fact, when investigating reactions that degrade complex lignin

polymers as a substrate, it is essential to consider the effect of lignin composition, sub-structure, and cross-linking on selective degradation. For instance, higher content of ether linkages such as β-O-4, α-O-4, 4-O-5 in different types of lignin enhances bio-oil generation and lignin depolymerization.[9] Moreover, the lignin composition and abundance of β-O-4 linkages can affect the distribution of products (e.g., non-alkylated phenolic derivatives versus alkylated phenolic derivatives).[10] Thus, the fact that different types of lignin result in different degradation products further complicating understanding of the degradation process.

Transformation of lignin into useful chemicals can be accomplished through a variety of thermochemical processes divided into four categories: pyrolysis, hydrolysis, hydrogenolysis, and oxidation.[11, 12] Oxidation can occur with enzymes, molecular oxygen, hydrogen peroxide, ozone, or other oxidative radical species. The oxidation modification of lignin typically adds functional groups to the aromatic rings, and as a result alcohol, aldehyde and acid derivatives can be obtained including phenol, guaiacol, hydroxybenzaldehyde, vanillin, and syringaldehyde, along with various carboxylic acids.[13-16] These natural aromatic compounds can be utilized as building blocks for polymer and bisphenols, polyesters, polyurethane, and resins.[17] Additionally, lignin degradation products as green feedstock have applications in carbon fiber, plastics, and elastomers, which help reducing dependency on fossil fuel-derived products.[18] Alternatively, low molecular weight compounds such as acetic acids, aliphatic, and olefins can also be obtained during lignin deconstruction process.[17, 19] However, the isolation and purification of these lignin products are challenging and still require extensive research.

Among oxidation methods, little progress has been made toward radical initiated

selective degradation of lignin.[7, 20] Lignin oxidation can occur on aliphatic OH, phenolic OH, or lignin benzylic positions.[21] For the efficient utilization of lignin, it is crucial to understand the correlation between radicals chemistry and lignin structural features. In this study, it is hypothesized that reactive oxygen species can selectively react with lignin due to their unique properties, half-life time, and redox potential.[22] To test the hypothesis, this study aimed to illustrate radical species reaction patterns on breaking C–O–C and C–C bonds of lignin to decipher their mechanisms in the oxidative cleavage. Four reactive species including superoxide anion radical ($O_2^{\bullet-}$), sulfate radical ($SO_4^{2-\bullet}$), hydroperoxide anion (HO_2^-), and hydroxyl radical ($HO^\bullet$) were studied. These reactive species are either known or suspected to play a role in efficient lignin degradation in a biological system, yet their mechanism of action has not been thoroughly examined.[23] The results of the study are expected to provide new insights to understanding these processes.

Materials and methods

Overview

Two lignin sources, milled lignin (ML) as a representative native lignin source and Kraft lignin (KL) as a by-product of the pulping process, were used in this study. Milled lignin was extracted and purified under mild conditions, while Kraft lignin had modified structure due to degradation that occurred during the pulping process when it was treated at elevated temperature with a mixture of NaOH and Na_2SO_4. During this process, Kraft lignin hydroxyl groups became sulfonated that could affect the reactivity.[24] Kraft lignin was also soluble in alkaline solution, whereas milled lignin suffers from lack of solubility. From reaction point of view, these differences may change the degradation pathway during oxidation and product distribution. Thus, it is

vital to investigate the reaction patterns of these two lignin types for comparison purposes.

The milled and Kraft lignins were oxidized by superoxide radical anion, sulfate radical, hydroperoxyl anion, and hydroxyl radical. Functional group modification, chemical structural changes, molecular weight deviations, rings and side-chain alteration, and lignin thermal stability were analyzed with a series of instruments including Fourier transform infrared spectroscopy (FTIR), gel permeation chromatography (GPC), pyrolysis-gas chromatography/mass spectrometry (Py-GC/MS), heteronuclear single quantum coherence spectroscopy (HSQC), and thermo-gravimetric analysis (TGA/DTG). The overall organization of the experimental work of this study is illustrated in ***Figure 1***.

The oxidation reaction explored in this study were water-based where oligomer rich compounds were separated, precipitated, and recovered by pH adjustment and dialysis followed by solvent extraction. Purification and identification of these monomers was not within the scope of this study. The goal of selective oxidation of lignin is to reach high yields of target products. Nonetheless, further separation and purification of the products obtained may be still necessary since most of the chemical industries prefer pure raw materials.

Materials and Chemicals

Kraft lignin with low contents of sulfonate, tetrahydrofuran (THF), 1,4-Dioxane, methanol, acetone, toluene, ethanol, chloroform, sodium persulfate, ferrous sulfate heptahydrate, and *N-tert*-butyldiethanol amine, was purchased from Sigma Aldrich (St. Louis, MO). Potassium superoxide was obtained from Acros (Branchburg, NJ).

Hydrogen peroxide and sodium perborate monohydrate were purchased from J.T. Baker (Phillipsburg, NJ). All chemicals were used without any further purification unless otherwise specified.

Isolation of lignin from wheat straw

Lignin Isolation was accomplished by ball-milling according to the procedure shown in ***Figure 2***. Among the many different lignin isolations, the one proposed by Bjorkman in 1957[25] is considered to yield material most representative of native lignin with few structural modification.[26, 27] Thus, Milled lignin in this study was prepared accordingly through a series of solvent extractions, followed by physical milling of the biomass, and subsequently by dissolution steps to purify the lignin derived from the starting material. Wheat straw was sieved through 30 mesh and dried before any extraction steps then added to an appropriate glass microfiber extraction thimble. Extraction was performed with Soxhlet using 9:1 acetone:water (v/v) at their boiling point for a minimum of 8 h to remove extraneous components.[7] A second extraction step was performed after the methanol wash of biomass with 2:1 ethanol:toluene (v/v) overnight. Biomass was air dried after extraction steps for 8 h to remove ethanol/toluene followed by further drying at 50 °C overnight. Dry biomass was milled in the planetary ball mill with ceramic milling jars for 48 h at ~550 RPM with a 15 minute on/off cycle. Lignin dissolution was performed in dioxane:water (DW) (96:4, 10 mL DW/g biomass) for 24 h at 50 °C. The top liquid was transferred into Teflon centrifuge tubes and centrifuged at 10,000 rpm for 10 min at 4 °C. After removing the dioxane by rotary evaporator, the residue was collected as milled lignin. The overall yield of ML was 5% by mass of the original starting material (wheat straw).[25]

The purchased Kraft lignin was purified by 24 h chloroform wash, and then subjected to

our radical oxidation study to compare degradation pathways between the two sources of lignins.

Lignin oxidation by $O_2^{\bullet-}$, $SO_4^{2-\bullet}$, HO_2^-, and $HO^\bullet$ reactive oxygen species

150 mg of each milled and Kraft lignin was oxidized separately at room temperature for 3 h in 20 mL aqueous solution of 0.05 mM oxidation reagents including superoxide radical anion ($O_2^{\bullet-}$)[28], sulfate radical ($SO_4^{2-\bullet}$)[29], hydroperoxide anion (HO_2^-)[30], and hydroxyl radical($HO^\bullet$)[31]. The radical species were generated via oxidative reagents decompactions in potassium superoxide (PS), sodium persulfate (SP), sodium perborate (PB), and iron (II) catalyzed hydrogen peroxide (FE) systems, respectively. These oxidations methods were the same as those reported elsewhere.[23]

After 5 h of reaction, the generated derivative compounds were extracted by chloroform to be evaluated by GC/Mass for identification, and the remaining solid part was dialyzed to separate oligomer-rich from any salts or unseparated chemicals. After 48 h of dialysis, the lignin solution was freeze-dried and the solid residue was separated.

Lignin Acetylation

Prior to all GPC studies, the solubility of lignin sample (50 mg) in THF was improved by acetylation in 1:1 pyridine/acetic anhydride v/v at 50 °C for 24 h according to the reported procedure.[32] After this time, acetylated lignin was precipitated after the addition of ether to the crude reaction mixture. The precipitated lignin was then collected and washed three times with deionized water leading to acetylated lignin.

Dialysis

Lignin samples were added to Thermo Scientific Snake Skin 3.5 K MWCO dialysis membrane tube and soaked in 1 L deionized water to remove any remaining salts or

polysaccharide residue. The membrane was left in the water at room temperature for 24 h, then the contents of the dialysis tubing was freeze-dried and the oligomeric lignin residue was obtained.

Fourier transform infrared spectroscopy (FTIR)

FTIR analysis was conducted to study changes of functional groups and structure in the oxidized lignin. ATR-FTIR spectra were obtained on a Shimadzu IR-Prestige FTIR spectrophotometer with 64 scans in absorbance mode. Samples were analyzed from 600 to 4000 cm^{-1} at a resolution of 8 cm^{-1}.

Gel permeation chromatography (GPC)

The weight-average molecular weight (*Mw*), number-average molecular weight (*Mn*) and polydispersity index (*PDI*, *Mw*/*Mn*) of lignin samples were determined by GPC equipped with 2 mixed bed 4.6 mm× 300 mm Styragel Waters Column. Samples were acetylated via the procedure above prior to the GPC analysis. Acetylated lignin sample (10 mg /mL in THF) was then analyzed using a Fisher Dionex Ultimate GPC system with a refractive index detector at 40 °C and THF as eluent with a flow rate of 1.0 mL/min. The column system was calibrated with a set of monodisperse polystyrene standards.

Pyrolysis Gas Chromatography-Mass Spectrometry (Py-GC/MS)

To validate the degradation of aromatic lignin moieties and examine changes in H, G, and S units of the lignin structure in the raw and radical-oxidized samples, pyrolysis analysis was carried out. Pyrolysis was conducted using a CDS 5000 pyrolysis autosampler connected to an Agilent GC/MS system for 56 min. 5 mg of control and radical-oxidized lignin were loaded into a packed quartz tube and pyrolyzed at 610 °C

for 1 min. Different pyrolytic products were separated by a (5%-phenyl)-methylpolysiloxane non-polar column with a 30 m×25 mm inner diameter and analyzed using a mass spectrometer (Inert XL MSD). The abundance of each pyrolyzed product was normalized against the area of CO_2 as an internal standard.

Heteronuclear single quantum coherence spectroscopy (HSQC)

Samples of milled and Kraft lignins (~50 mg), both control and radical-oxidized, were dissolved in DMSO-d_6. 700 μL of each sample solution was transferred to a 5 mm NMR tube and recorded by using 256 increments and 32 scans per increment at 30 °C. A hetero-2D single quantum correlation (adiabatic pulse sequence, HSQCAD) NMR spectrum was acquired on a Varian/Agilent 600 MHz VNMRS DD2 NMR spectrometer. The spectrometer was equipped with a two-channel-optimized H-X autotuning probe (Agilent OneProbe) and Z-axis gradients. A T2 filter (CPMGT2, Tau=25 ms) was incorporated to avoid line broadening interference from high molecular weight polymeric lignin. Data were acquired in F2 (^{1}H) with a spectral width of 9615.4 Hz, and the acquisition time of 150 ms, and 1442 complex points. The F1 (^{13}C) sweep width was 30154.5 Hz. NMR spectra were deduced by using MestRenova software.

Thermo-gravimetric analysis (TGA/DTG)

To analyze the thermal behavior of the radical-oxidized and control lignin samples, TGA and DTG were performed on a TGA/SDTA 851 thermogravimetric analyzer using a Mettler Star system equipped with STARE data analysis software. Approximately 5 mg of sample was heated in a weighting crucible with the heating rates of 10 °C/min to 900 °C and a flow rate of 20 mL/min under a nitrogen atmosphere in duplicate.

Results and discussion

FTIR analysis of wheat straw following oxidative pretreatment

The FTIR spectra of lignin and oxidized lignin for both milled and Kraft lignin are depicted in ***Figure 3***. The strong absorbance at 3300-3600 cm^{-1} indicative of the hydroxyl groups in carboxylic, phenolic, and alcoholic subunits of lignin was present in both control and treated samples.[33] This band lessened in almost all samples compared to control, attributing to the removal of phenolic units in lignin. Comparatively, oxidized milled lignin by FE method showed an intensified hydroxyl group peak, which was interpreted as more hydroxyl group formation and oxidation of lignin side chains. The peak at 2800-2950 cm^{-1} known as the =C–H and C–H stretching vibration decreased in SP, PB, and FE-oxidized milled and Kraft samples. The decrease in =C–H and C–H peaks of bamboo lignin treated with radical oxidation has been also observed by others and referred to demethoxylation and demethylation.[34] The aforementioned stretching vibrations did not alter in the PS-oxidized milled sample but increased in the Kraft lignin sample, indicating extra free C–H groups after treatment. The peak at 1655-1800 cm^{-1} assigned to the carbonyl stretching vibration diminished in PS and PB treated samples and increased in SP and FE-oxidized milled and Kraft samples due to the side-chain oxidation and β-O-4 linkage cleavage (which were proved by Py-GC/MS and HSQC).[35] The PS, SP and FE-oxidized milled lignin showed a significant increase in aromatic C–C stretching at 1600 cm^{-1} which indicated more free aromatic rings after oxidation. In addition, PS oxidation led to more free aromatic ring in Kraft samples, SP and FE showed lower peak intensity at 1500-1650 cm^{-1}, indicating the difference of milled and Kraft lignin structures. Oxidized milled and Kraft lignins by PB methods didn't show any notable changes in aromatic region which indicated that this method

was not effective enough for lignin linkages breakage (also confirmed by high *Mw* by GPC).

Moreover, the band assigned to guaiacyl groups at 1270 cm^{-1} showed lower intensity for PS and PB methods, meaning that oxidation methods decreased the G unit content of lignin (also validated by Py-GC/MS) which have been observed in other studies.[21] Methoxy peak at 1330 and 1110 cm^{-1} (C–H in-plane deformation of S unit) increased in both SP and FE oxidized milled and Kraft samples, whereas this peak appeared with lower intensity in PS and PB methods. The moderated intensities of methoxy-substituted units of lignin in oxidized samples indicated that syringyl (S), guaiacyl (G), and p-hydroxyphenylpropane (H) units were separated from lignin after oxidation[36], which suggested that S units were converted to G units via demethoxylation expressly in PS method. Removal of S unit peaks alongside with the presence of G unit C–H correlation peaks in HSQC also supported this interpretation. Aliphatic OH and ether groups bands appeared at 1030-1090 cm^{-1} were increased in the SP and FE-oxidized samples. Oxidative cleavage of lignin phenylpropanoid units which are connected with α-O-4 and β-O-4 linkages can generate aldehydes, ketones, and carboxylic acids groups.[37] The higher quantity of oxygen-containing groups in this method was also observed in Py-GC/MS and HSQC measurements.

Molecular weight analysis of lignin by GPC

The weight-average, number average molecular weights, and polydispersity determined by GPC analysis are presented in ***Table 1.*** The results indicated the degree of lignin depolymerization. Before oxidation, the acetylated milled lignin showed the *Mw* of 4.6 kDa, consistent with literature *Mw* of milled lignin ranging from 3.0 to 5.0 kDa.[38, 39] After PS oxidation, *Mw* shifted to 1.0 kDa. This indicates that lignin depolymerized by

forming low molecular weight compounds (this was also confirmed by GC/MS data which was not shown here). The same trend of reduction in *Mw* was observed for SP (1.3 kDa), PB (2.2 kDa), and FE (2.3 kDa)-oxidized milled lignin but with a lower degree than that for PS method. For all samples, one peak with lower *Mn* compared to control was observed. Similar results were also obtained in lignin oxidation by different transition metals under oxidizing conditions of H_2O_2.[21] *Mn* showed to be lower for PS (0.8 kDa) and SP (0.7 kDa) as compared to milled lignin (1.9 kDa). However, the PB (1.3 kDa) and FE (1.5 kDa) showed higher *Mn* values compared to PS and SP methods. The polydispersity decreased from milled lignin (2.42) to PS (1.25), SP (1.85), PB (1.69), and FE (1.53), indicating transition from a wide span of *Mw* in milled lignin toward more specific oligomers of lignin after oxidation. Low *Mw* lignin is identified to be more reactive toward further reactions compared to high *Mw* samples.[40]

Mw of acetylated Kraft lignin was 3.0 kDa while it changed to 1.2 kDa following reaction via SP. The *Mw* of PB and FE-KL exhibited the values of 3k and 1.6 kDa. PS method did not show any significant peak in GPC trace (or the monomer peaks was buried under the solvent peak), which is a sign of extensive lignin depolymerization. The reduction in *Mn* and *Mw* indicates that the lignin molecules were fragmented into smaller units. Cleavage of ether and carbon-carbon linkages can lead to low molecular weight lignin, which contains oxygen-containing groups.[38] The polydispersity of Kraft lignin was changed from 2.72 to 1.33, 1.76, and 1.06 in SP, PB, and FE-oxidized treatments, separately, which means a narrow distribution of the molecular weight of lignin sample after the treatment.

Taken together, although the results illustrated the significant degradation with the PS method, moderate degradation with PS, and low degradation with PB and FE methods,

oxidized lignin can undergo re-polymerization as have been seen in our GPC data for PB-treated Kraft lignin and reported by others.[21, 41-43] Lignin condensation reaction or repolymerization is a common phenomenon in oxidation systems.[44] However, based on GPC trace the final Mw was lower than the untreated sample, even though repolymerization occurred for radical treated samples. As can be seen from the Py-GC/MS and TGA results, lignin degradation generated some complex structures due to radical-radical re-combination. These produced compounds have lower Mw compared to untreated lignin but higher thermal stability.

Py-GC/MS study of lignin pyrolysis and the effect of oxidation methods on product distribution

Py-GC/MS analysis can provide a better understanding of the lignin modification during oxidation at the structural level.[45] Lignin is anticipated to degrade into small fragments after pyrolysis which then can be separated and identified by gas chromatography and mass spectrometry.[46] The resulted chromatogram (pyrogram) constitutes a fingerprint of the starting polymer, which provides information on the number of monomeric subunits.[47] ***Table 2*** lists the pyrolysis products abundance and their corresponding retention time, which was used to create H, G, and S contents presented in ***Table 3***. The percentage of H unit of milled lignin (***Table 3***) changed from 8.70% in control to 43.71%, 10.42%, 56.73%, and 9.93% in PS, SP, PB, and FE-oxidized lignin, separately. The relative abundance of G unit was 61.97%, 56.29%, 69.32%, 21.43%, and 61.59% for milled lignin, PS, SP, PB, and FE, correspondingly. It is in agreement with the reduction of 1270 cm^{-1} (guaiacyl absorbance band in FTIR) in PS and PB methods, which indicates the cleavage of lignin linkages.[38, 48] It is important to point out that according to the Py-GC/MS data, the number of G units increased in the SP method.

Similarly, FTIR data showed an increase in SP-oxidized sample absorbance band of guaiacyl groups. S unit of milled lignin revealed 29.33% abundance whereas the oxidized samples by PS did not show any S residue in Py-GC/MS pyrogram. SP, PB, and FE exhibited 20.25%, 21.84%, and 28.48% S-derived compounds, separately. Samuel et al. declared that lignin depolymerization is feasible by breaking the β-O-4 linkage in the S unit.[4, 49] Moreover, it is reported that lignin oxidation by other oxidation agents such as ozone led to S unit degradation.[50] S unit degradation is feasible by homolytic methoxy bond cleavage, and catechol intermediate formation followed by dehydration to be converted to guaiacols or phenols units.[51] Taken together this implies that the results in this study are consistent with the observation by others that G units are more resistant to oxidation than S units. The preferential removal of S unit is due to the lower redox potential of S unit than G unit, that makes it less recalcitrant towards oxidative breakdown.[52]

The S/G ratio in PS, SP, PB, and FE-oxidized lignin decreased from 0.47 in control to 0.00, 0.29, 1.02, and 0.46, respectively. A decrease in lignin S/G ratio makes substrate degradation easier, which was also reported in oxidative biological treatment.[53]

Phenol, a representative of H units, appeared at a retention time of 8.65 min of the pyrogram. The abundance of phenol increased after oxidation from 2.76% in control to 8.26%, 4.66%, 18.37%, and 3.39% (% of total phenolic-derived compounds area) in PS, SP, PB, and FE-oxidized samples, separately. The phenolic lignin derivatives were dominant in spectra such as 2-methoxy phenol (G unit), 2-methoxy-4-methyl phenol (G unit), 4-ethyl-2-methoxy phenol (G unit), 2-methoxy-4-vinyl phenol (G unit), and 2, 6-dimethoxy phenol (S unit), 2-methoxy-4-propyl phenol (G unit), vanillin (G unit), 3-methoxy-1,2-benzenediol (G unit), 2-methoxy-4-(2-propenyl) phenol (G unit), etc.

observed at 11.22, 13.71, 15.68, 16.61, 17.48, 17.65, 18.74, 18.91, and 19.52 min, respectively. The abundance of phenolic compounds with one or no methoxy substituent in the pyrogram showed that the H and G-units were higher in oxidized samples than S-lignin units. The increase in 2-methoxy phenol by 273.89% and 8.43% (% of total phenolic-derived compounds area) in PS and SP, respectively, is a sign of loosely packed lignin morphology because of carbon-carbon cleavage. This phenolic derivative decreased by 10.29% and 9.56% in PB and FE-oxidized milled lignin, indicating lignin ring demethylation.

The abundance of carbonyl functionality on C_α or C_β of pyrolytic products such as 4-hydroxy-3-methoxy benzene acetic acid (retention time of 23.29 min) in SP and FE-oxidized samples was the main difference with PS and PB methods, which is a sign of C_β–Cγ cleavage in SP and FE methods. Two new compounds appeared in Py-GC/MS trace of the PS-oxidized sample at 16.22 min (3,4-dihydro-3,3,6,8-tetramethyl-1(2H)-naphthalenone) and 18.84 min (2-benzoyl-1-naphthalene carboxylic acid) which indicated lignin polymer condensation through radical-radical reaction.

The generation of large amount of acids, ketone, and aldehydes compounds such as benzaldehyde (7.85 min), acetophenone (10.52 min), vanillin (18.74 min), 1-(2,6-dihydroxy-4-methoxyphenyl) ethanone (20.40 min), 4-hydroxy-3-methoxy benzoic acid methyl ester (20.87 min), 2,4'-dihydroxy-3'-methoxy acetophenone (22.31 min), 4-hydroxy-3-methoxy benzene acetic acid (23.29 min), 4-hydroxy-2-methoxycinnamaldehyde (29.25 min), etc. in SP and FE-oxidized samples agrees with lignin side-chain oxidation. The characteristic absorption of C=O peaks in the FTIR spectra of SP and FE methods further supports the observation. These results reflect lignin substructure degradation and side-chains hydroxyl groups oxidation that are in

agreement with a similar study on oxidized lignin pyrolysis.[36, 54] Some of the generated monomers such as vanillin can be utilized directly without any further upgrading. However, some phenolic derivatives need transformations to target products which is challenging.[55]

This data suggest that the oxidation of lignin involved syringyl unit degradation and the oxidation of the side chain of guaiacyl unit. These observations agree with previous studies in termite where Katsumata et al.[56] and Geib et al.[45] found that the lignin oxidation pathway is via propyl side-chain oxidation (depolymerization), demethylation of ring methoxyl group, and ring hydroxylation.

Lignin structure and interunit linkages analysis by HSQC

HSQC analysis was intended to obtain structural information by monitoring C–H correlations. HSQC of milled and Kraft radical-treated samples were evaluated and annotated in ***Figure 4*** and ***Figure 5***. The aliphatic and aromatic region appeared in δ_C/δ_H 10–120/1.0–5.5 ppm and δ_C/δ_H 100–135/5.5–8.0 ppm, respectively. The lignin substructures and signal assignments are listed in ***Figure 6*** and ***Table 4***, respectively.

The HSQC spectra of control milled lignin sample contained signals corresponding to C_α–H_α in G (δ_C/δ_H 71.78/4.68 ppm) and S (δ_C/δ_H 72.20/4.80 ppm) type units, C_β–H_β in H (δ_C/δ_H 84.76/4.24 ppm), G (δ_C/δ_H 86.29.78/4.06 ppm), and S (δ_C/δ_H 86.86/4.15 ppm) type units, and C_γ–H_γ (δ_C/δ_H 60.18/3.35 and 3.64 ppm) correlations in β-aryl ether (β-O-4) substructure. The cross signal of C_α–H_α, C_β–H_β, and C_γ–H_γ corresponded to phenyl coumaran substructure appeared at δ_C/δ_H 87.26/5.41, 55.72/3.35, and 63.32/3.33 ppm, separately. The other major signals in the aliphatic region belonged to resinol, dibenzodioxocins, spirodienones, coniferyl alcohol, cinnamyl aldehyde, p-coumarate,

and ferulate substructures. The aromatic region of the milled lignin HSQC spectra corresponding to H (weak signal for $C_{2,6}$–$H_{2,6}$ and $C_{3,5}$–$H_{3,5}$), G (strong signal for C_2–H_2 and $C_{5,6}$–$H_{5,6}$), and S (prominent signal for $C_{2,6}$–$H_{2,6}$) units showed signal in range of δ_C/δ_H 100/7.0 ppm in agreement with earlier HSQC studies of wheat straw milled lignin.[57, 58] Compared to control, PS-oxidized milled lignin signal for C_α–H_α, and C_β–H_β in β-aryl ether linkages of S type subunit disappeared as well as the correlated peaks of S substructure, which indicated that the method precisely affects β-aryl ether substructure of S type. This suggests that meta-substituted units were modified by PS oxidation.[59] S unit degradation in lignin was also reported when wheat straw lignin was oxidized by ozone.[50]

Removal of S unit was further confirmed with the Py-GC/MS results showing that S unit of lignin diminished in pyrogram spectra after oxidation of lignin with PS method. It is important to point out that the PS method did not degrade β-aryl ether G type substructure since the correlated peaks of α, β, and ɣ C–H were the major signals in the spectra. Moreover, the correlations for C_α–H_α, and C_β–H_β phenyl coumarin substructure were not observed in PS method while the weak correlated peak of C_γ–H_γ still existed in the spectra showing that the sigma bond in C_α–C_β position changed to double bond. This result is reasonable since the appearance of vinylic peaks (δ_C/δ_H 95–105/4.7–5.5 ppm) in 2D HSQC of PS samples was one of the significant changes of the spectra of this method compared to that of the milled lignin. Remarkably, the C_α/H_α correlations at δ_C/δ_H 154.73–7.61 ppm and C_β/H_β correlations at δ_C/δ_H 127.16–6.87 ppm of cinnamyl aldehyde (I) substructure with vinyl carbon-carbon double bond was measured with higher intensity in PS method. It is worth mentioning that in untreated milled lignin, the cinnamyl aldehyde (I) substructure signals was observed in HSQC spectra [60]. In

addition, phenylcoumaran (B) depleted peaks can be elucidated by depolymerization pathway that occurred between C_α–C_β. The cleavage started via dehydrogenation followed by bond homolysis forming dihydrobenzofuran and 2-methoxy phenol, as illustrated in ***Figure 7***.[61] Interestingly, dihydrobenzofuran and 2-methoxy phenol with a retention time of 14.55 and 11.22 min, respectively, were the primary pyrolysis products peaks identified with a considerable level in PS-oxidized lignin. The control milled lignin did not show any trace of dihydrobenzofuran after pyrolysis. Depolymerization mechanism in phenylcoumaran subunits was studied experimentally and theoretically through bond dissociation energy (BDE) by Lou et al.[61] Cleavage of phenylcoumaran substructure through C_α–$C_{aromatic}$ linkage was supported experimentally and by BDE since BDE of C_α–$C_{aromatic}$ bond is lower than C_α–O linkages.

The correlated peaks of C–H in milled lignin resinol (C) substructure was not distinguished after oxidation by PS methods, as well as the associated correlation of S units peaks. Resinol substructure oxidation by superoxide radical leads to hydroxy methoxy phenol derivative via oxidative side-chain replacement (***Figure 7***).[37] Resinol units degradation was also reported by[62-64] in which phenolic aldehydes and ketones were the major reaction products after catalytic oxidation (***Figure 7***, second route).[37]

The H lignin unit produced strong correlations in the PS-oxidized sample for $C_{2,6}$–$H_{2,6}$ at δ_C/δ_H 128.48/7.13 ppm, and $C_{3,5}$–$H_{3,5}$ at δ_C/δ_H 115.41/6.70 ppm along with G lignin unit for C_2–H_2 at δ_C/δ_H 111.14/6.91 ppm, and $C_{5,6}$–$H_{5,6}$ at δ_C/δ_H 115.0/6.63 ppm. These findings were also confirmed with Py-GC/MS methods in which these two subunits were abundant in the lignin after oxidation. The above data confirmed that the lower S/G ratio is an important factor for lignin degradation and the S unit is easier to be degraded or modified by oxidation method.[65] Lignin methoxy group removal by free

radicals were also reported in other studies[51] where lignin was degraded by free radical in pyrolysis. The degradation pathway involved phenoxy radical formation by removing hydrogen atom of S unit followed by ipso rearrangement (***Figure 7***). In this way, S unit can be converted to guaiacol and its derivatives.[66]

For the SP-oxidized milled lignin, the most abundant linkages were phenyl coumarin (B), resinol (C), H, G, and S (weak signals) substructures. However, the correlated peaks of β-aryl ether (A) linkages in this sample were almost completely absent which means that this method selectively breaks α–β linkage according to ***Figure 7***. Studies on fungal lignin degradation showed propyl side-chain oxidation followed by C_α–C_β cleavage, which formed different derivatives of methoxy benzoic acid.[45] This means that α–β cleavage by SP method led to the generation of oxidized side-chain products as illustrated by carbonyl peaks in FTIR spectra and side-chain oxidized monomers in Py-GC/MS pyrogram. The removal of β-aryl ether (A) substructures from SP-oxidized lignin can also be correlated to β-O-4 linkages cleavage which also led to the formation of oxygen-containing products as depicted in ***Figure 7***.[37] Comparing β-O-4 and C–C bonds, it can be perceived that the ether bond is easier to be cleaved.[67] Relatively, the corresponding peaks of C_α–H_α, and C_β–H_β in dibenzodioxocins substructure (D) at δ_C/δ_H 83.73/4.26 and 86.57/4.03 ppm, respectively were absent in the SP-oxidized sample. The low abundance of dibenzodioxacin substructure was also observed in lignin, which was extracted from treated wheat straw by *P. chrysosporium* (white-rot fungi).[68] As shown in ***Figure 7***, degradation can start by homolytic cleavage of both C_α of ether linkages to produce carbonyl derivatives.[69] This mechanism was also confirmed by Cogulet et al.[69] where white spruce was degraded by UV irradiation. The degradation started by the radical attack and homolytic cleavage of both C_α of dibenzodioxocin unit

ether linkage which in turn generated bierol and coniferyl alcohol compounds (***Figure 7***).

Moreover, spirodienones (E) substructure peaks were disappeared after SP oxidation indicating that SP-ML has a low content of β-1′ and α-O-α′ linkages due to radical oxidation which formed the carbonyl derivatives products.[70, 71] Spirodienone unit degradation screening has also been studied by molecular dynamics to distinguish possible products and linkages cleavage.[71] The depolymerization pathway of ether and C–C bond in spirodienone unit is energetically favorable which further validates the proposed deconstruction pathway in this work.

Moreover, new peaks appeared in the region of carbinyls groups (oxygenated products) at δ_C/δ_H 70–80/2.8–3.5 ppm which suggests condensation reaction and re-polymerization via phenoxy radical formation and radical cross-linking coupling.[51] Interestingly the correlated peaks of C_γ–H_γ in oxidized guaicyl structure (G′) detected in SP-oxidized sample illustrated the preference of this method to oxidize the α position of G substructure. Although the decreased amount of S unit was detected in SP-oxidized sample, no trace of oxidized S unit was measured in the HSQC spectra.

Taken together, these results indicate that superoxide radical, a strong nucleophile with low redox potential (-0.2 V) oxidize lignin via cleavage of C–C bonds of lignin by nucleophilic addition, while sulfate radical with high redox potential initiated oxidative cleavage of lignin by β-O-4 breakage.[23, 72] C–C and C–O bonds cleavage result in benzene, toluene, xylene, and phenol products which can be further purified and utilized. In addition, selective lignin depolymerization results in some compounds which can be hardly obtained by conventional petrochemical process.[73, 74]

The same trend of degradation was identified in Kraft samples. Kraft lignin is different from milled lignin since the Kraft lignin structure had already been degraded to some degree and it contained more hydrophilic groups compared to milled lignin.[75] The aliphatic and aromatic regions of Kraft lignin contained the corresponding signals of aryl ether, phenylcoumaran, resinol, cinnamyl alcohol, cinnamyl aldehyde, p-coumarates, ferulate, secoisolariciresinol, aryl enol ether, p-hydroxyphenyl, guaiacyl units, guaiacyl hydroxyethyl ketone, guaiacyl propanol, and syringyl substructures. Some new substructures were found in Kraft lignin samples, which is typical since this lignin already went through Kraft process and is expected to show oxidized side-chain.[76] For both milled and Kraft lignin oxidized by PS method, evidence for degradation of resinol substructures (C) linkages was not observed, while by SP method the β-aryl ether substructure was removed.

An acceptable 2D spectra of PB and FE-oxidized lignins was unfortunately could not obtain during the study, although enormous efforts were made, such as changing the experimental method, removing residual metals, increasing the lignin concentration in DMSO-d_6, increasing the number of increments, etc. It was believed that the remaining trace of salts in the lignin structure resulted in diminished HSQC signals, most likely due to exchange processes, dielectric effects on tuning, and potentially from the reformation of high molecular weight lignin from reactive cleaved product lignin units under the conditions of the reaction. For these samples, 1-D H-NMR spectra clearly showed the aromatic region's peaks. However, the correlated peaks could not be captured in HSQC due to the low signal to noise ratio.

It is important to remark that lignin depolymerization usually resulted in complex product mixtures that need to be purified and upgraded to final chemicals. However, the

complexity of the lignin and the generated products mixture are limiting factors toward lignin biorefinery. The efficient separation and purification of lignin-based chemicals are critical for biorefinery development.[55] The first phase for lignin valorization is finding advanced deconstruction procedures for depolymerization. When the first goal is achieved, an effective separation and purification of product mixtures must be investigated and evaluated. In this study, a green radical deconstruction approaches was proposed to break different lignin linkages. Further study is required to identify product distribution and further transformations.

Thermogravimetric analysis (TGA/DTG) of milled and Kraft lignin

The TGA and DTG curves of milled and Kraft lignin before and after oxidation are shown in ***Figure 8***. Thermal degradation of lignin complex structures can occur under a wide temperature range due to its side chains and a variety of functional groups.[32] Any weight loss below 120 °C was considered as the moisture content in samples. Major decomposition occurred from 150 °C to 790 °C. Milled lignin showed two representative DTG peaks between 150 °C and 450 °C due to the cleavage of the lignin side chain and β-O-4 linkage which is consistent with the literature.[36, 77] Decomposition of Kraft lignin occurred as one peak at 315 °C resulted from the partially degraded structure of this kind of lignin. These results are in accordance with GPC analysis, in which the *Mw* of milled lignin was higher than Kraft lignin. PS-oxidized lignin shifted decomposition peaks to lower temperatures (232 °C and 335 °C) with a significant amount of second peak mass loss (50%). According to GPC, the thermal stability of the oxidized lignin decreased with decreasing *Mw*. PB-oxidized sample had higher *Mw* compared to PS which led to higher decomposition at 316 °C and 672 °C. Interestingly, the peaks of SP and FE samples were observed at higher temperatures. A possible

explanation is the formation of modified fragments through a condensation reaction, which leads to structures with more stability and higher decomposition temperature.[41] Besides, lignin dissociation in these two methods occurred as two peaks: at lower temperature 250-290 °C and high temperature 630-750 °C. The high decomposition temperature observed in the SP and FE methods originated from C–C cleavage bonds in highly condensed lignin.[32] The thermal degradation of Kraft lignin oxidation by these radicals proceeded the same pattern unlike in Kraft lignin the mass quantity of the peaks was lower compared to milled lignin due to the nature of Kraft lignin. PS-oxidized Kraft lignin had the lowest decomposition rate and highest weight loss which is in accordance with GPC data. Moreover, it is known that β-O-4 linkages in-between S units of lignin are easier to cleave than β-O-4 linkages in G units. Based on the Py-GC/MS data, the S to G ratio of milled and Kraft lignin decreased in the order of PS, SP, FE, and PB. These results indicated that the thermal stability of PS sample was the lowest among all oxidation methods and that the small β-O-4 peak (290-390 °C) was the sign of S type β-O-4 linkages oxidation in this method.

The results confirm that radical species generated different distributions of products and therefore had different reaction mechanisms. For example, superoxide radical ion preferred partially positive charged parts of lignin and could modify lignin by nucleophilic addition. The highly reactive radical, sulfate radical reacted with electron-rich sites on lignin. Another feature of the sulfate radical is that it has relatively long half-life time (~ minutes), especially compared to hydroxyl radical. Hydroperoxide anion could attack the electron-deficient parts of biomass[78], and finally, hydroxyl radical, a short lifetime radical with high redox potential, can react with double bonds and aromatic rings.[72, 79-82] The lignin depolymerization mechanism obtained from FTIR,

GPC, Py-GC/MS, HSQC, and TGA/DTG showed that superoxide radical anion selectivity break β-β and β-5 linkages, thus can be used for the vinyl aromatic and phenolic compounds production. In contrast, sulfate radical has high capability to degrade lignin from β-O-4 linkages which can produce aromatic aldehydes, aromatic ketones, and aromatic carboxylic acids. The oxidative pattern of hydroperoxide anion and hydroxyl radical resulted in almost the same trend of reaction as superoxide radical anion and sulfate radical, respectively. However, further study is required to specify their reaction mechanism in breaking lignin inter-unit linkages, as well as determining conditions that optimize their performance. It needs to be emphasized that, although the identification and utilization of some end products from lignin were discussed carefully by others[74], utilization of the radical degradation products as the mixture is very complex and enormous amount of research is required to investigate the valorization and upgrading process of generated aromatic intermediates after lignin depolymerization.[73]

Conclusion

The reaction of Milled and Kraft lignins with superoxide, sulfate, hydroperoxide, and hydroxyl radicals were investigated. Reactions with these oxidative species changed the functional groups and the weight average molecular weight of lignin and reduced S/G subunit ratios. β-β and β-5 cleavage of lignin aromatic rings occurred by superoxide radical anion, while the sulfate radical depolymerized lignin by removing β-O-4 linkages. This work provided new insights into radical reactivity toward lignin linkages and illustrated the mechanism through which each oxidation method degraded lignin. The information is beneficial for developing rational commercial processes to make value-added products from lignin.

Conflicts of interest

There are no conflicts to declare.

Acknowledgments

This material is based upon work supported by Washington State University and the National Science Foundation under Grant No. 1231085. Preparation of the manuscript was supported by the USDA National Institute of Food and Agriculture, McIntire-Stennis Project WNP00009.

References

1. C. Bio-energy, 1984.
2. R. B. Santos, E. A. Capanema, M. Y. Balakshin, H.-M. Chang and H. Jameel, *Journal of Agricultural and Food Chemistry*, 2012, **60**, 4923-4930.
3. E. A. Capanema, M. Y. Balakshin and J. F. Kadla, *Journal of agricultural and food chemistry*, 2005, **53**, 9639-9649.
4. X. L. Qiao, C. Zhao, Q. Shao and M. Hassan, *Energy Fuels*, 2018, **32**, 6022-6030.
5. M. Brebu and C. Vasile, *Cellulose Chemistry and Technology*, 2010, **44**, 353-363.
6. M. D. Krks, B. S. Matsuura, T. M. Monos, G. Magallanes and C. R. J. Stephenson, *Org. Biomol. Chem.*, 2016, **14**, 1853-1914.
7. H. Lange, S. Decina and C. Crestini, *European Polymer Journal*, 2013, **49**, 1151-1173.
8. J. J. Bozell, J. O. Hoberg and D. R. Dimmel, *Tetrahedron Letters*, 1998, **39**, 2261-2264.
9. J. Park, A. Riaz, R. Insyani and J. Kim, *Fuel*, 2018, **217**, 202-210.
10. F. P. Bouxin, A. McVeigh, F. Tran, N. J. Westwood, M. C. Jarvis and S. D. Jackson, *Green Chem.*, 2015, **17**, 1235-1242.
11. C. Amen-Chen, H. Pakdel and C. Roy, *Bioresource Technology*, 2001, **79**, 277-299.
12. D. W. Ribbons, *Philosophical Transactions of the Royal Society of London. Series A, Mathematical and Physical Sciences (1934-1990)*, 1987, **321**, 485-494.
13. A. L. Mathias, M. I. Lopretti and A. E. Rodrigues, *Journal of Chemical Technology & Biotechnology*, 1995, **64**, 225-234.
14. H.-R. Bjørsvik and F. Minisci, *Organic Process Research & Development*, 1999, **3**, 330-340.
15. S. Ramachandra Rao and G. A. Ravishankar, *Journal*, 2000, **80**, 289-304.
16. M. Fache, B. Boutevin and S. Caillol, *ACS Sustainable Chemistry & Engineering*, 2016, **4**, 35-46.

17. K. Davis, M. Rover, R. Brown, X. Bai, Z. Wen and L. Jarboe, *Energies*, 2016, **9**, 808.
18. A. J. Ragauskas, G. T. Beckham, M. J. Biddy, R. Chandra, F. Chen, M. F. Davis, B. H. Davison, R. A. Dixon, P. Gilna, M. Keller, P. Langan, A. K. Naskar, J. N. Saddler, T. J. Tschaplinski, G. A. Tuskan and C. E. Wyman, *Science (New York, N.Y.)*, 2014, **344**, 1246843-1246843.
19. J. Zakzeski, P. C. A. Bruijnincx, A. L. Jongerius and B. M. Weckhuysen, *Chemical reviews*, 2010, **110**, 3552-3599.
20. A. Das, A. Rahimi, A. Ulbrich, M. Alherech, A. Motagamwala, A. Bhalla, L. Sousa, V. Balan, J. Dumesic, E. Hegg, B. Dale, J. Ralph, J. Coon and S. S. Stahl, *ACS Sustain. Chem. Eng.*, 2018, **6**, 3367-3374.
21. L. Das, S. Xu and J. Shi, *Frontiers in Energy Research*, 2017, **5**.
22. G. R. Buettner, *Arch Biochem Biophys*, 1993, **300**, 535-543.
23. M. Davaritouchaee, W. C. Hiscox, J. Martinez-Fernandez, X. Fu, R. J. Mancini and S. Chen, *Industrial Crops & Products*, 2019, **137**, 484-494.
24. J. Gierer, *Journal of the International Academy of Wood Science*, 1980, **14**, 241-266.
25. A. Bjorkman, *Industrial & Engineering Chemistry*, 1957, **49**, 1395-1398.
26. A. Guerra, I. Filpponen, L. A. Lucia, C. Saquing, S. Baumberger and D. S. Argyropoulos, *Journal of agricultural and food chemistry*, 2006, **54**, 5939-5947.
27. J. R. Obst and T. K. Kirk, *Methods in Enzymology*, 1988, **161**, 3-12.
28. S. Marklund, *The Journal of biological chemistry*, 1976, **251**, 7504.
29. O. S. Furman, A. L. Teel and R. J. Watts, *Environmental Science & Technology*, 2010, **44**, 6423-6428.
30. M. D. David and J. N. Seiber, *Environmental Pollution*, 1999, **105**, 121-128.
31. S. Y. Jeong and J. W. Lee, *Bioresource Technology*, 2016, **200**, 121-127.
32. J.-Y. Kim, S. Oh, H. Hwang, U.-J. Kim and J. W. Choi, *Polymer Degradation and Stability*, 2013, **98**, 1671.
33. A. Tejado, C. Peña, J. Labidi, J. M. Echeverria and I. Mondragon, *Bioresource Technology*, 2007, **98**, 1655-1663.
34. K. Wu, W. Ying, Z. Shi, H. Yang, Z. Zheng, J. Zhang and J. Yang, *ACS Sustain. Chem. Eng.*, 2018, **6**, 3853-3861.
35. X. Chen, H. Li, S. Sun, X. Cao and R. C. Sun, *Scientific Reports*, 2016, **6**.
36. L. Xiaona, S. Shujuan, T. Shun, U. P. Charles, S. Jianping and Z. Zhijun, *Energies*, 2015, **8**, 5107-5121.
37. R. Ma, M. Guo and X. Zhang, *Catalysis Today*, 2018, **302**, 50-60.
38. A. H. G. Mohammadali Azadfar, Mahesh V. Bule, Shulin Chen, *International Journal of Biological Macromolecules*, 2015, **75**, 58–66.
39. J. Zeng, G. L. Helms, X. Gao and S. Chen, *Journal of agricultural and food chemistry*, 2013, **61**, 10848-10857.
40. A. Pizzi, *Advanced wood adhesives technology*, 1994.
41. J. Li, G. Henriksson and G. Gellerstedt, *Lignin depolymerization/repolymerization and its critical role for delignification of aspen wood by steam explosion*, 2007, **98**, 3061-3068.
42. R. El Hage, N. Brosse, L. Chrusciel, C. Sanchez, P. Sannigrahi and A. Ragauskas, *Polymer Degradation and Stability*, 2009, **94**, 1632-1638.
43. A. Toledano, L. Serrano and J. Labidi, *Fuel*, 2014, **116**, 617-624.
44. K. H. Kim and C. S. Kim, *Frontiers in Energy Research*, 2018, **6**.

45. S. M. Geib, T. R. Filley, P. G. Hatcher, K. Hoover, J. E. Carlson, M. M. Jimenez-Gasco, A. Nakagawa-Izumi, R. L. Sleighter and M. Tien, *Proceedings of the National Academy of Sciences*, 2008, **105**, 12932.
46. B. Yang and C. E. Wyman, *BSA treatment to enhance enzymatic hydrolysis of cellulose in lignin containing substrates*, 2006, **94**, 611-617.
47. J. J. M. Órfão and F. G. Martins, *Thermochimica Acta*, 2002, **390**, 195-211.
48. J. M. Lawther, R. Sun and W. B. Banks, *Fractional characterization of wheat straw lignin components by alkaline nitrobenzene oxidation and FT-IR spectroscopy*, 1996, 1241-1247.
49. R. Samuel, Y. Pu, B. Raman and A. Ragauskas, *Part A: Enzyme Engineering and Biotechnology*, 2010, **162**, 62-74.
50. M. V. Bule, A. H. Gao, B. Hiscox and S. Chen, *Journal of agricultural and food chemistry*, 2013, **61**, 3916.
51. M. Lei, S. Wu, J. Liang and C. Liu, *Journal of Analytical and Applied Pyrolysis*, 2019, **138**, 249-260.
52. A. T. Martínez, S. Camarero, A. Gutiérrez, P. Bocchini and G. C. Galletti, *Journal of Analytical and Applied Pyrolysis*, 2001, **58**, 401-411.
53. J. I. Hedges, K. Weliky and A. H. Devol, *Geochimica et Cosmochimica Acta*, 1988, **52**.
54. V. Gvozdev and É. Chupka, *Chemistry of Natural Compounds*, 1983, **19**, 487-489.
55. C. Xu, R. A. D. Arancon, J. Labidi and R. Luque, *Chem. Soc. Rev.*, 2014, **43**, 7485-7500.
56. K. S. Katsumata, Z. Jin, K. Hori and K. Iiyama, *Journal of Wood Science*, 2007, **53**, 419-426.
57. J. C. Del Río, J. Rencoret, P. Prinsen, Á. T. Martínez, J. Ralph and A. Gutiérrez, *Journal of agricultural and food chemistry*, 2012, **60**, 5922.
58. C. Crestini and D. S. Argyropoulos, *Structural analysis of wheat straw lignin by quantative 31P and 2D NMR spectroscopy. The occurrence of ester bonds and alpha-O-4 substructures*, 1997, **45**, 1212-1219.
59. S. Constant, H. L. J. Wienk, A. E. Frissen, P. D. Peinder, R. Boelens, D. S. Van Es, R. J. H. Grisel, B. M. Weckhuysen, W. J. J. Huijgen, R. J. A. Gosselink and P. C. A. Bruijnincx, *Green Chem.*, 2016, **18**, 2651-2665.
60. Y. Pu, F. Chen, A. Ziebell, B. Davison and A. Ragauskas, *BioEnergy Research*, 2009, **2**, 198-208.
61. R. Lou, G. Lyu, S. B. Wu, B. Zhang, H. Zhao and L. Lucia, *ACS Sustain. Chem. Eng.*, 2018, **6**, 430-437.
62. H. Deng, L. Lin and S. Liu, *Energy & Fuels*, 2010, **24**, 4797-4802.
63. H. Deng, L. Lin, Y. Sun, C. Pang, J. Zhuang, P. Ouyang, J. Li and S. Liu, *Energy & Fuels*, 2009, **23**, 19-24.
64. F. G. Sales, L. C. A. Maranhão, N. M. Lima Filho and C. A. M. Abreu, *Industrial & Engineering Chemistry Research*, 2006, **45**, 6627-6631.
65. J.-L. Wen, B.-L. Xue, F. Xu, R.-C. Sun and A. Pinkert, *Industrial Crops & Products*, 2013, **42**, 332-343.
66. M. Asmadi, H. Kawamoto and S. Saka, *Journal of Analytical and Applied Pyrolysis*, 2011, **92**, 88-98.
67. J. Chen, C. Liu, S. Wu, J. Liang and M. Lei, *RSC Adv.*, 2016, **6**, 107970-107976.
68. D. Singh, J. Zeng, D. D. Laskar, L. Deobald, W. C. Hiscox and S. Chen,

Biomass and Bioenergy, 2011, **35**, 1030-1040.
69. A. Cogulet, P. Blanchet and V. Landry, *Journal of Photochemistry & Photobiology, B: Biology*, 2016, **158**, 184-191.
70. B. Jiang, Y. Zhang, T. Guo, H. Zhao and Y. Jin, *Polymers*, 2018, **10**.
71. B. D. Mar and H. J. Kulik, *The journal of physical chemistry. A*, 2017, **121**, 532-543.
72. M. Davaritouchaee and S. Chen, *Biomass and Bioenergy*, 2018, **116**, 249-258.
73. A. Ricardo, P.-A. Heriberto and C. Leonardo, *Processes*, 2018, **6**, 98.
74. J. E. Holladay, J. F. White, J. J. Bozell and D. Johnson, *Journal*, 2007.
75. E. Sjoestroem, *Wood chemistry: fundamentals and applications*, Academic Press, Inc.,New York, NY, 1981.
76. C. Crestini, H. Lange, M. Sette and D. S. Argyropoulos, *Green Chem.*, 2017, **19**, 4104-4121.
77. S. Chu, A. V. Subrahmanyam and G. W. Huber, *Green Chem.*, 2013, **15**, 125-136.
78. A. T. Quintanilha, *Reactive oxygen species in chemistry, biology, and medicine*, Plenum Press, New York, 1988.
79. H. Zemel and R. W. Fessenden, *The Journal of Physical Chemistry*, 1978, **82**, 2670-2676.
80. D. T. Sawyer, *Oxygen chemistry*, New York ; Oxford, England : Oxford University Press, New York ; Oxford, England, 1991.
81. D. T. Sawyer, J. J. Stamp and K. A. Menton, *The Journal of Organic Chemistry*, 1983, **48**, 3733-3736.
82. S. Kobayashi, T. Tezuka and W. Ando, *Journal of the Chemical Society, Chemical Communications*, 1979, 508-510.
83. J. Ralph, T. Akiyama, H. Kim, F. Lu, P. Schatz, J. Marita, S. Ralph, M. Reddy, F. Chen and R. Dixon, *Journal of Biological Chemistry*, 2006, **281**, 8843-8853.
84. R. F. Helm and J. Ralph, *Lignin-hydroxycinnamyl model compounds related to forage cell wall structure. 1. Ether-linked structures*, 1992, 2167-2175.

Figure captions:

Figure 1: Schematic diagram for the experimental procedure of milled and Kraft lignins oxidation by $O2^{\bullet-}$, $SO4^{2-\bullet}$, $HO2^{-}$, and $HO^{\bullet}$ species, degraded lignin isolation by solvent extraction and dialysis, and lignin characterization by NMR, GPC, FTIR, Py-GC/MS, and TGA

Figure 2: The scheme of the milled lignin production process from wheat straw started with biomass chips size reduction, followed by pre-extraction and ball milling then lignin content of biomass obtained after dissolving in dioxane

Figure 3: FTIR spectra of the milled and Kraft lignin before and after oxidation by $O2^{\bullet-}$, $SO4^{2-\bullet}$, $HO2^{-}$, and $HO^{\bullet}$ species

Figure 4: 2D-NMR HSQC spectrum (in DMSO-d6) of milled lignin (ML) sample and oxidized samples by $O2^{\bullet-}$ (PS-ML) and $SO4^{2-\bullet}$ (SP-ML) species. The color of the cross peak indicates the phase. CH and CH3 appear as red and CH2 has a blue color. The circles indicate the major difference of spectra with control

Figure 5: 2D-NMR HSQC spectrum (in DMSO-d6) of Kraft lignin sample (KL) and oxidized samples by $O2^{\bullet-}$ (PS-KL) and $SO4^{2-\bullet}$ (SP-KL). The circle indicates the major difference of spectra with control

Figure 6: Lignin substructure identified by 2D-NMR HSQC to show assigned lignin linkages: (A) aryl ether; (B) phenylcoumaran; (C) resinol; (D) dibenzodioxocins; (E) spirodienones; (F) cinnamyl alcohol end-groups; (I) cinnamyl aldehyde end-groups; (J) p-coumarates; (K) ferulate; (L) secoisolariciresinol; (M) aryl enol ether; (N) stilbene; (H) p-hydroxyphenyl; (G) guaiacyl; (G') guaiacyl hydroxyethyl ketone; (G'') guaiacyl propanol; (S) syringyl57, [76]

Figure 7: Possible lignin degradation pathway in oxidation systems and the generated monomers37, [51, 61, 69, 71]

Figure 8: TGA and DTG for four Milled and Kraft lignins before and after oxidation (heating rate of 10 °C/min). Lignin structures degradation under a wide temperature range due to its side chains and a variety of functional groups.

Table 1: Average molecular weights and polydispersity of control and oxidized Kraft lignin (ND=not determined). ML: milled lignin, KL: Kraft lignin, PS: oxidation by superoxide radical via potassium superoxide decomposition, SP: oxidation by sulfate radical via sodium persulfate decomposition, PB: oxidation by hydroperoxide anion via sodium perborate decomposition, and FE: oxidation by hydroxyl radical via Fenton reaction

Sample (Acetylated)	Weight Average *Mw (g/mol)*	Number Average *Mn (g/mol)*	Polydispersity *PDI*
Milled lignin	4600	1900	2.42
PS-ML	1000	800	1.25
SP-ML	1300	700	1.85
PB-ML	2200	1300	1.69
FE-ML	2300	1500	1.53
Kraft lignin	3000	1100	2.72
PS-KL	ND	ND	ND
SP-KL	1200	900	1.33
PB-KL	3000	1700	1.76
FE-KL	1600	1500	1.06

Table 2: Percentages of pyrolysates from the control and radical treated of Milled lignin and radical-oxidized samples. The pyrogram gives information about the lignin monomeric components at different retention time

No.	Name	Molecular Formula	Retention Time (min)	Peak Assignment	ML (%)	PS (%)	SP (%)	PB (%)	FE (%)
1	Benzaldehyde	C_7H_6O	7.853		0.300	0.000	0.540	0.690	0.700
2	Phenol	C_6H_6O	8.659	H	1.030	0.440	0.550	3.380	0.440
3	Benzene, 1-methoxy-4-methyl-	$C_8H_{10}O$	9.307		0.090	0.080	0.000	0.350	0.000
4	Benzene, 1-ethenyl-4-methyl-	C_9H_{10}	9.656		0.000	0.000	0.000	0.140	0.000
5	Phenol, 2-methyl-	C_7H_8O	10.402	H	0.950	0.360	0.000	3.850	0.520
6	Acetophenone	C_8H_8O	10.523		0.130	0.000	0.230	0.000	0.000
7	Phenol, 2-methoxy-	$C_7H_8O_2$	11.222	G	1.780	0.950	0.610	0.787	0.560
8	Benzene, 1,2-dimethoxy	$C_8H_{10}O_2$	12.495		0.000	0.330	0.000	0.880	0.000
9	Benzene, 1-ethenyl-4-methoxy-	$C_9H_{10}O$	12.607		0.000	0.330	0.000	0.000	0.000
10	Phenol, 2,4-dimethyl-	$C_8H_{10}O$	12.637	H	0.390	0.520	0.000	1.920	0.000
11	Phenol, 4-ethyl-	$C_8H_{10}O$	13.137	H	0.330	0.710	0.000	0.730	0.210
12	Naphthalene	$C_{10}H_8$	13.357		0.330	0.000	0.000	0.000	0.150
13	Phenol, 2-methoxy-4-methyl-	$C_8H_{10}O_2$	13.715	G	1.400	0.270	0.575	0.320	0.200
14	Phenol, 3,5-dimethyl-	$C_8H_{10}O$	13.81	H	0.070	0.000	0.000	0.400	0.000
15	Phenol, 2,3,6-trimethyl	$C_9H_{12}O$	14.013	H	0.000	0.190	0.000	0.160	0.000
16	Benzenecarboxylic acid	$C_7H_6O_2$	14.039		0.300	0.000	0.000	0.000	0.000
17	Benzofuran, 2,3-dihydro-	C_8H_8O	14.552		3.400	1.760	0.340	1.030	1.330
18	Phenol, 2-propyl-	$C_9H_{12}O$	15.471	H	0.000	0.110	0.000	0.000	0.000
19	Phenol, 4-ethyl-2-methoxy-	$C_9H_{12}O_2$	15.683	G	0.690	0.450	1.906	0.560	0.130
20	Naphthalene, 1-methyl-	$C_{11}H_{10}$	15.950		0.470	0.000	0.000	0.140	0.000
21	1(2H)-Naphthalenone, 3,4-dihydro-3,3,6,8 tetramethyl-	$C_{14}H_{18}O$	16.222		0.000	7.890	0.000	0.000	0.000
22	2-Methoxy-4-vinylphenol	$C_9H_{10}O_2$	16.619	G	3.500	0.000	0.190	1.040	1.020
23	Benzaldehyde, 4-hydroxy	$C_7H_6O_2$	18.426	H	0.480	0.000	0.680	0.000	0.000
24	Phenol, 2,6-dimethoxy	$C_8H_{10}O_3$	17.482	S	2.890	0.000	1.140	3.520	0.540
25	Phenol, 2-methoxy-4-propyl-	$C_{10}H_{14}O_2$	17.650	G	0.370	0.000	0.570	0.000	0.460
26	Benzene, 1,2,3-trimethoxy-5-methyl	$C_{10}H_{14}O_3$	18.577		0.000	0.230	0.000	0.460	0.000
27	Vanillin	$C_8H_8O_3$	18.741	G	3.38	0.000	0.680	0.000	1.670
28	1-Naphthalene carboxylic acid, 2-benzoyl-	$C_{18}H_{12}O_3$	18.845		0.000	0.490	0.000	0.000	0.000
29	1,2-Benzenediol, 3-methoxy-	$C_7H_8O_3$	18.914	G	0.440	0.000	0.000	0.000	0.000
30	Phenol, 2-methoxy-4-(1-propenyl)-	$C_{10}H_{12}O_2$	19.522	G	3.010	0.380	0.49	0.450	0.460
31	1,1'-Biphenyl, 4-methyl-	$C_{13}H_{12}$	20.243		0.090	0.000	0.000	0.000	0.000
32	Benzene, 1,2-dimethoxy-4-(1-propenyl)-	$C_{11}H_{14}O_2$	20.394		0.000	0.110	0.000	0.180	0.000
33	Ethanone, 1-(2,6-dihydroxy-4-methoxyphenyl)-	$C_9H_{10}O_4$	20.402		0.780	0.000	0.000	0.000	0.530
34	Benzoic acid, 4-hydroxy-3-methoxy-, methyl ester	$C_9H_{10}O_4$	20.872	G	0.230	0.000	0.350	0.000	0.210
35	2,4'-Dihydroxy-3'-methoxyacetophenone	$C_9H_{10}O_4$	22.313	G	0.480	0.000	0.590	0.000	0.680
36	Phenol, 2,6-dimethoxy-4-(2-propenyl)-	$C_{11}H_{14}O_2$	22.520	S	0.640	0.000	0.000	0.000	0.000
37	3-Hydroxy-4-methoxybenzoic acid	$C_8H_8O_4$	23.185	G	2.880	0.000	0.000	0.000	0.000
38	Benzeneacetic acid, 4-hydroxy-3-methoxy	$C_9H_{10}O_4$	23.297	G	0.080	0.000	1.610	0.000	2.050
39	Phenol, 4-(ethoxymethyl)-2-methoxy	$C_{10}H1_4O_3$	23.625	G	0.180	0.000	0.000	0.000	0.000
40	Benzaldehyde, 4-hydroxy-3,5-dimethoxy	$C_9H_{10}O_4$	23.957	S	2.950	0.000	0.000	0.070	0.000
41	4-((1E)-3-Hydroxy-1-propenyl)-2-methoxyphenol	$C_{10}H_{12}O_3$	24.052	G	2.560	0.000	0.000	0.000	0.000
42	Phenol, 2,6-dimethoxy-4-(2-propenyl)-	$C_{11}H_{14}O_3$	24.328	S	0.000	0.000	0.000	0.200	0.230
43	Ethanone, 1-(4-hydroxy-3,5-dimethoxyphenyl)-	$C_{10}H_{12}O_4$	25.255	S	2.390	0.000	0.460	0.230	1.310
44	3,5-Dimethoxy-4-hydroxyphenylacetic acid	$C_{10}H_{12}O_5$	25.795	S	0.810	0.000	0.000	0.000	0.270
45	Aspidinol	$C_{12}H_{16}O_4$	26.662	G	0.580	0.000	0.830	0.000	0.000
47	n-Hexadecanoic acid	$C_{16}H_{32}O_2$	28.680		1.110	0.000	4.170	2.180	5.210
48	3,5-Dimethoxy-4-hydroxycinnamaldehyde	$C_{11}H_{12}O_4$	29.254	S	1.270	0.000	0.790	0.000	0.810

Table 3: Comparison between H, G, and S units as well as syringyl/guaiacyl ratio in analytical pyrolysis of samples before and after oxidation. The table is prepared based on abundance of each unit in ***Table 2****.*

	Samples				
	ML	PS	SP	PB	FE
H+G+S	37.34	5.33	11.80	18.40	12.99
H%	8.70	43.71	10.42	56.73	9.93
G%	61.97	56.29	69.32	21.43	61.59
S%	29.33	0.00	20.25	21.84	28.48
S/G%	0.47	0.00	0.29	1.02	0.46

Table 4: Assignment of C–H correlation signals in HSQC spectra of milled lignin sample and oxidized samples by $O_2^{\bullet-}$, $SO_4^{2-\bullet}$, HO_2^-, and $HO^\bullet$ species[60, 67, 76, 83, 84]

δ_C/δ_H (ppm)	Assignments
	β-aryl ether substructure (A)
71.78/4.68	C_α/H_α (G)
72.20/4.80	C_α/H_α (S)
84.76/4.24	C_β/H_β (H)
86.29/4.06	C_β/H_β (G)
86.86/4.15	C_β/H_β (S)
60.18/3.35 & 3.64	C_γ/H_γ
	Phenylcoumarans substructure (B)
87.26/5.41	C_α/H_α
55.72/3.35	C_β/H_β
63.32/3.33	C_γ/H_γ
	Resinol substructure (C)
85.41/4.26	C_α/H_α
54.25/2.99	C_β/H_β
72.89/3.40 & 4.68	C_γ/H_γ
	Dibenzodioxocins substructure (D)
83.73/4.26	C_α/H_α
86.57/4.03	C_β/H_β
	Spirodienones substructure (E)
81.69/4.98	C_α/H_α
61.76/2.62	C_β/H_β
85.41/4.58	$C_{\alpha'}/H_{\alpha'}$
	Cinnamyl alcohol substructure (F)
129.25/6.36	C_α/H_α
129.25/6.15	C_β/H_β
62.13/4.07	C_γ/H_γ
	Cinnamaldehyde substructure (I)
154.73/7.61	C_α/H_α
127.16/6.84	C_β/H_β
	p-coumarates substructure (J)
146.74/4.85	C_α/H_α
114.49/6.23	C_β/H_β
130.51/7.44	$C_{2,6}/H_{2,6}$
115.58/6.67	$C_{3,5}/H_{3,5}$
	Ferulates substructure (K)
145.78/7.54	C_α/H_α
114.49/6.23	C_β/H_β
123.35/7.13	C_6/H_6

	Secoisolariciresinol substructure (L)
42.3/1.9	C_{β}/H_{β}
	Aryl enol ether substructure (M)
112.1/6.2	C_{α}/H_{α}
	Stilbene substructure (N)
128.63/7.1	C_{α}/H_{α}
128.0/7.09	C_{β}/H_{β}
	p-hydroxyphenyl substructure (H)
128.48/7.13	$C_{2,6}/H_{2,6}$
115.41/6.70	$C_{3,5}/H_{3,5}$
	Guaiacyl substructure (G)
111.14/6.91	C_2/H_2
115.0/6.63 & 119.48/6.75	$C_{5,6}/H_{5,6}$
	Guaiacyl hydroxyethyl ketone substructure (G')
22.59/1.21	C_{γ}/H_{γ}
	Guaiacyl propanol substructure (G'')
35.05/1.48	C_{α}/H_{α}
	Syringyl substructure (S)
104.68/6.63	$C_{2,6}/H_{2,6}$
56.2/3.67	Methoxyl group

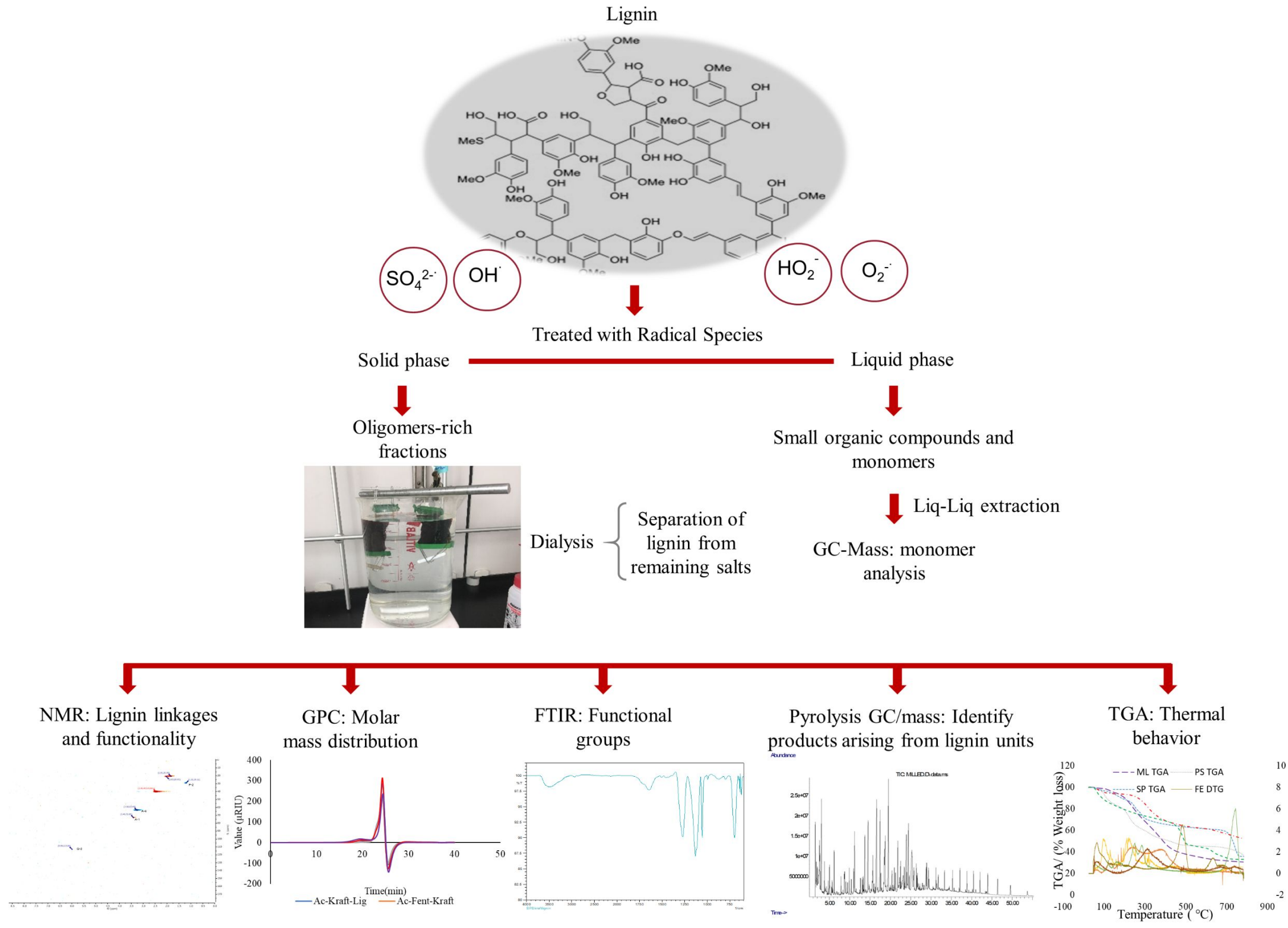

Figure 1: Schematic diagram for the experimental procedure of milled and Kraft lignins oxidation by $O_2^{\bullet-}$, $SO_4^{2-\bullet}$, HO_2^-, and $HO^{\bullet}$ species, degraded lignin isolation by solvent extraction and dialysis, and lignin characterization by NMR, GPC, FTIR, Py-GC/MS, and TGA

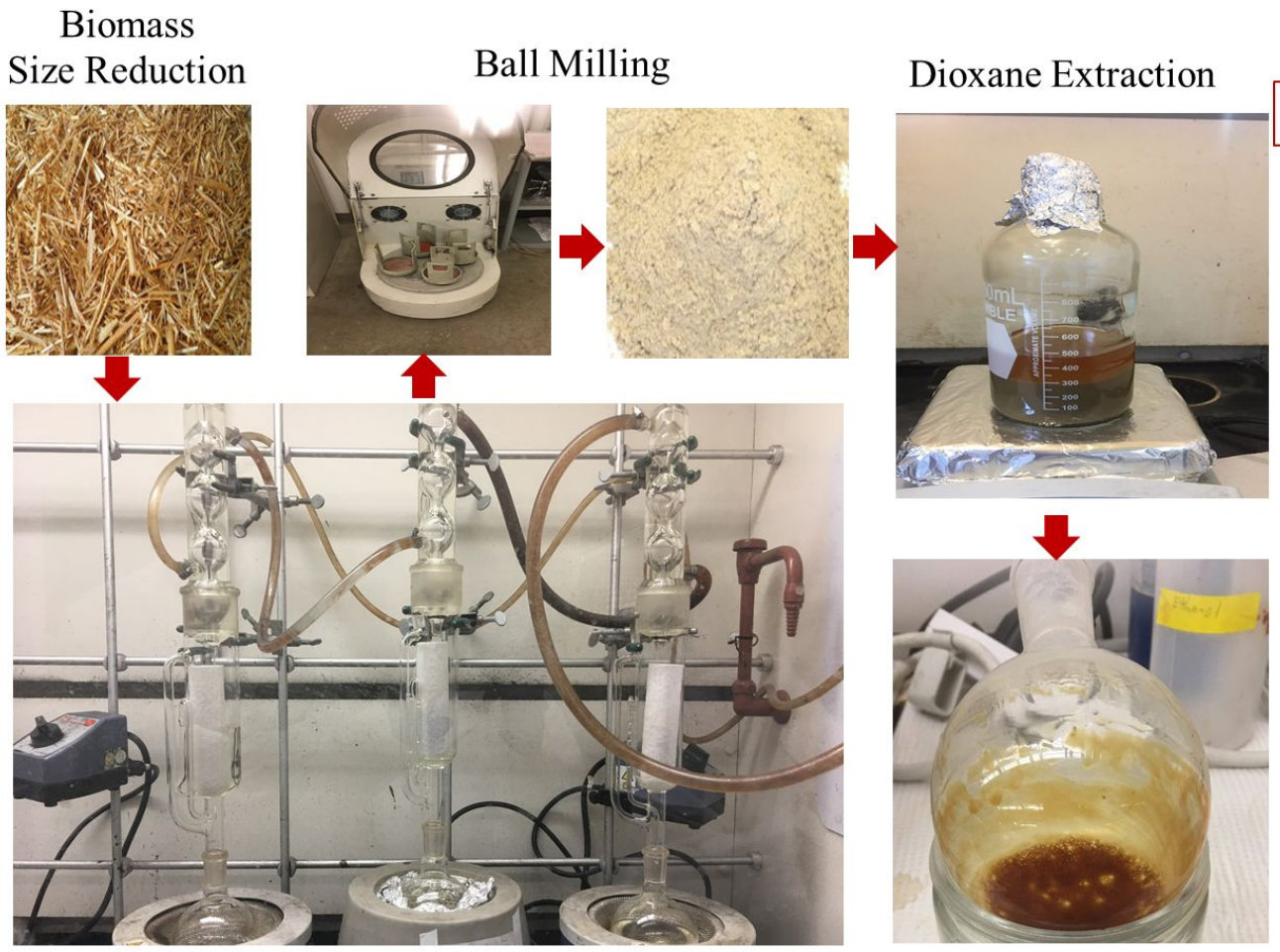

Figure 2: The scheme of the milled lignin production process from wheat straw started with biomass chips size reduction, followed by pre-extraction and ball milling then lignin content of biomass obtained after dissolving in dioxane

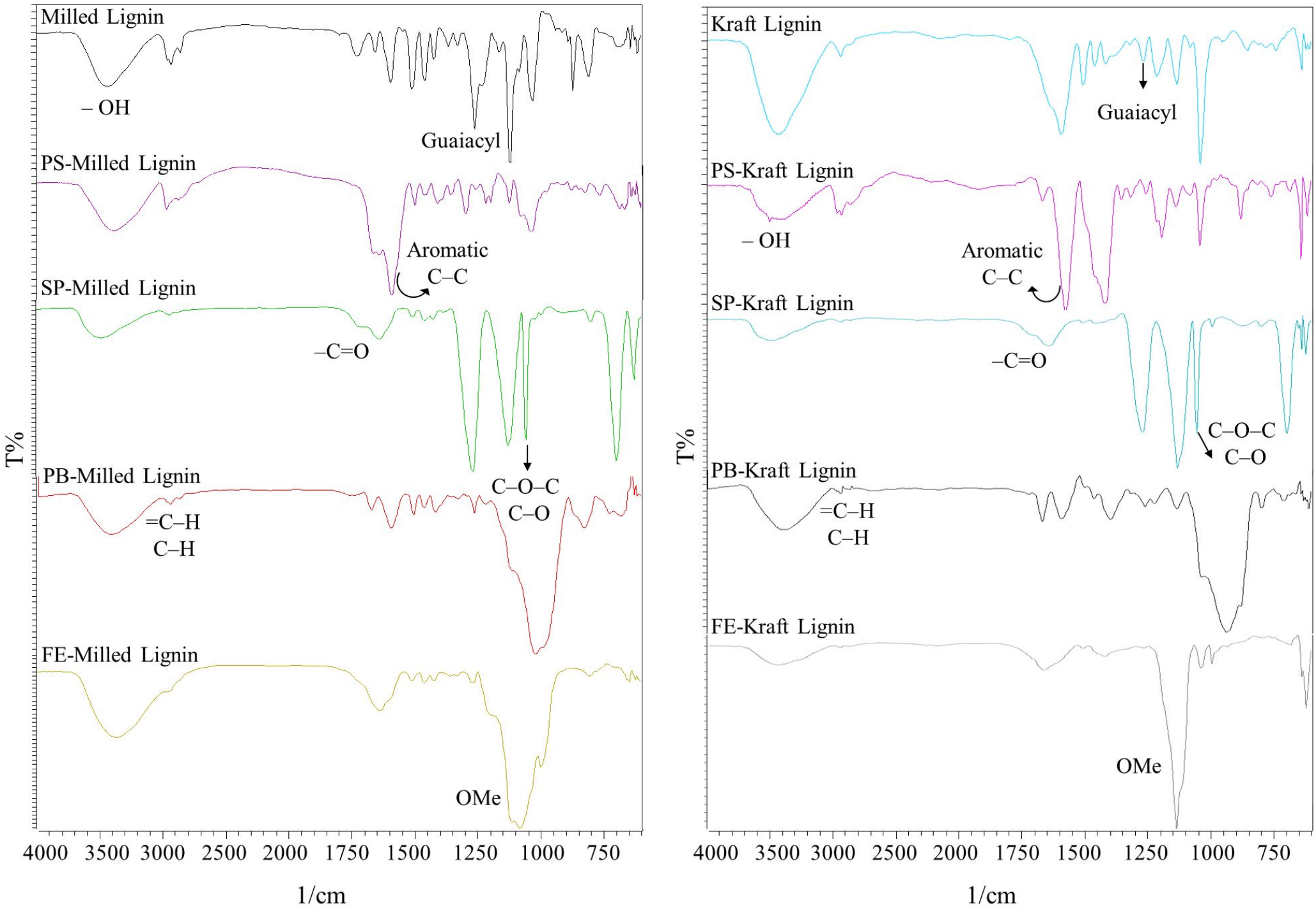

Figure 3: FTIR spectra of the milled and Kraft lignin before and after oxidation by $O_2^{\bullet -}$, $SO_4^{2-\bullet}$, HO_2^-, and $HO^\bullet$ species

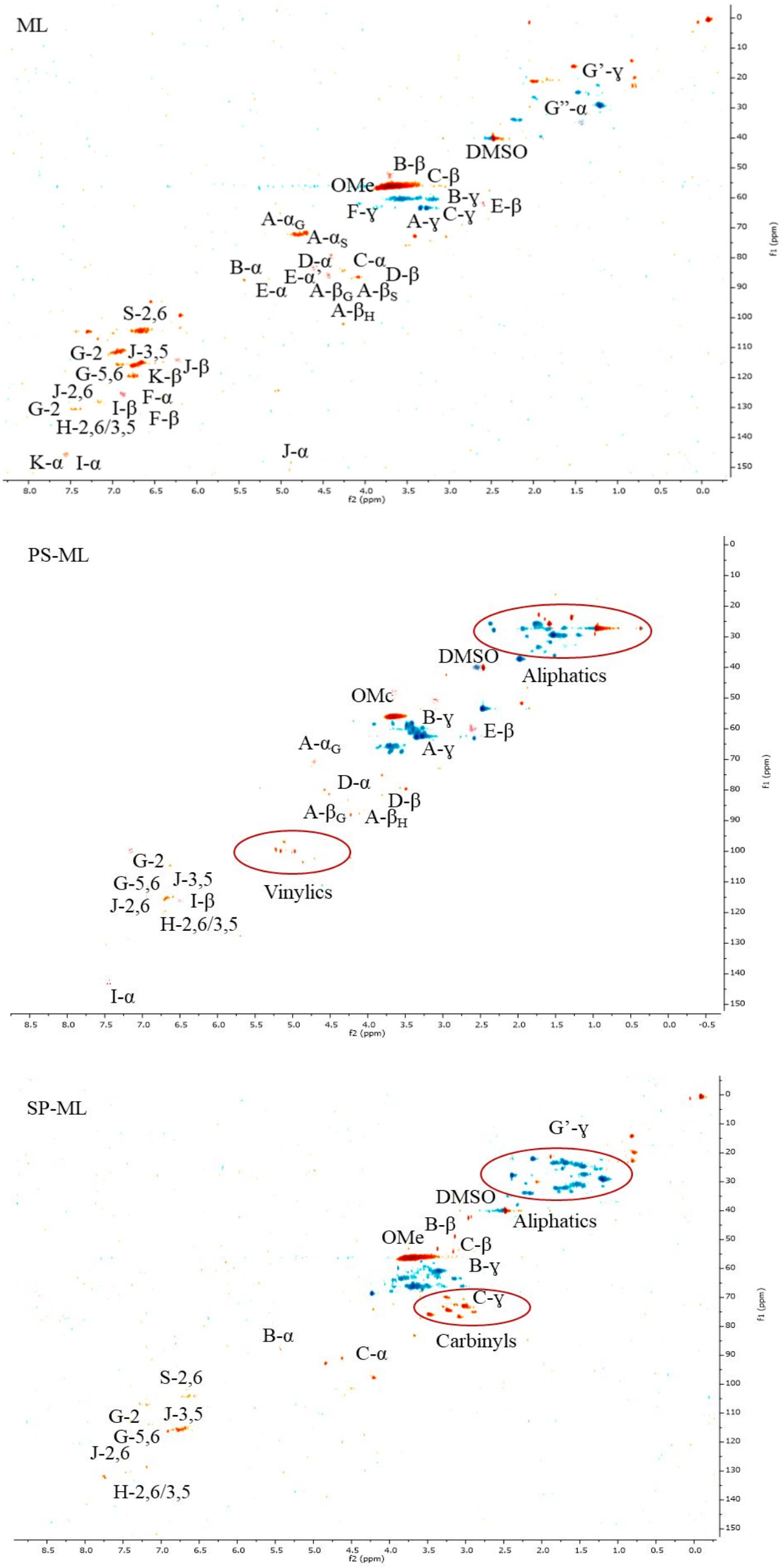

Figure 4: 2D-NMR HSQC spectrum (in DMSO-d6) of milled lignin (ML) sample and oxidized samples by $O_2^{\bullet-}$ (PS-ML) and $SO_4^{2-\bullet}$ (SP-ML) species. The color of the cross peak indicates the phase. CH and CH_3 appear as red and CH_2 has a blue color. The circles indicate the major difference of spectra with control

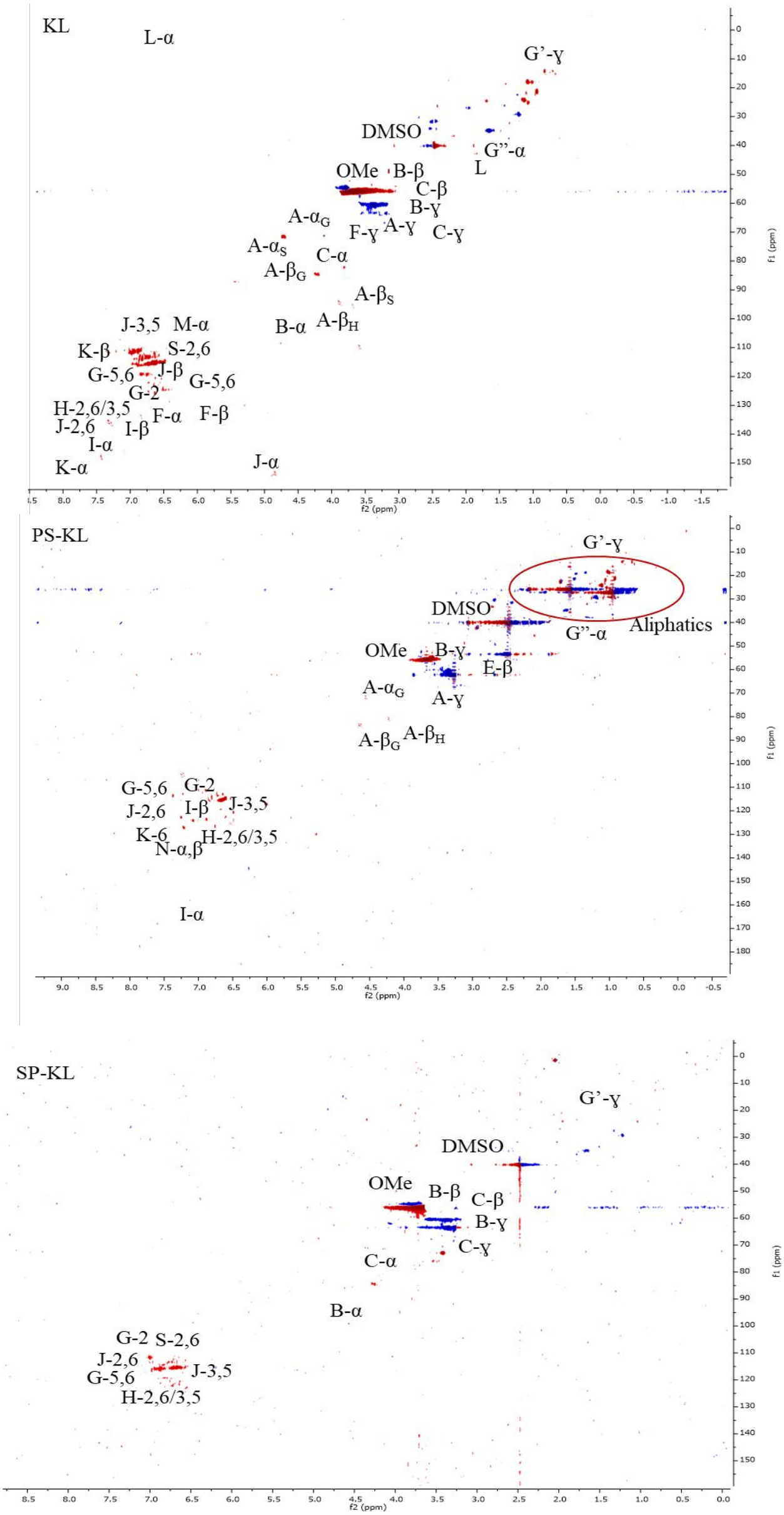

Figure 5: 2D-NMR HSQC spectrum (in DMSO-d6) of Kraft lignin sample (KL) and oxidized samples by $O_2^{\bullet-}$ (PS-KL) and $SO_4^{2-\bullet}$ (SP-KL). The circle indicates the major difference of spectra with control

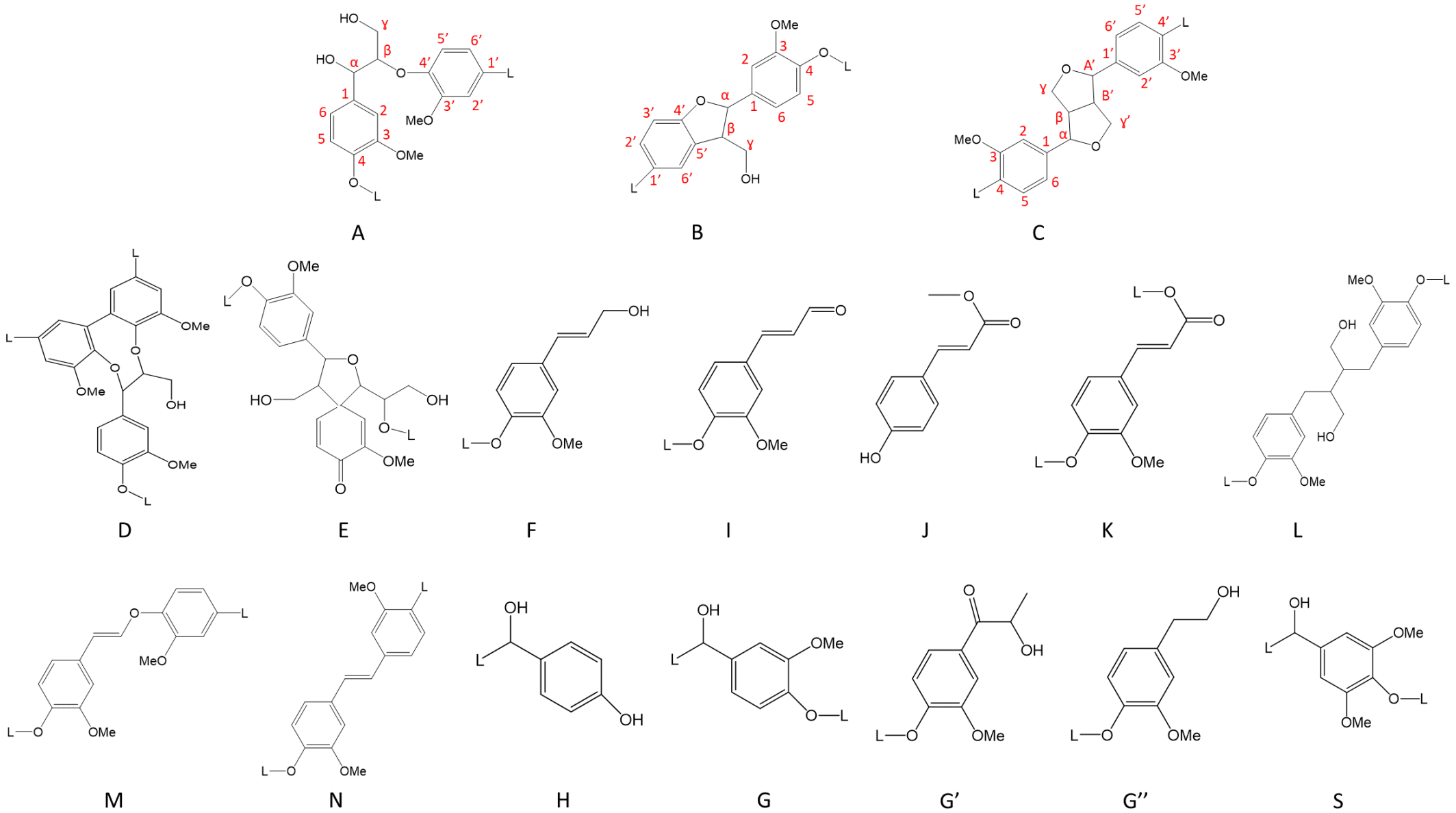

Figure 6: Lignin substructure identified by 2D-NMR HSQC to show assigned lignin linkages: (A) aryl ether; (B) phenylcoumaran; (C) resinol; (D) dibenzodioxocins; (E) spirodienones; (F) cinnamyl alcohol end-groups; (I) cinnamyl aldehyde end-groups; (J) p-coumarates; (K) ferulate; (L) secoisolariciresinol; (M) aryl enol ether; (N) stilbene; (H) p-hydroxyphenyl; (G) guaiacyl; (G’) guaiacyl hydroxyethyl ketone; (G’’) guaiacyl propanol; (S) syringyl[57, 76]

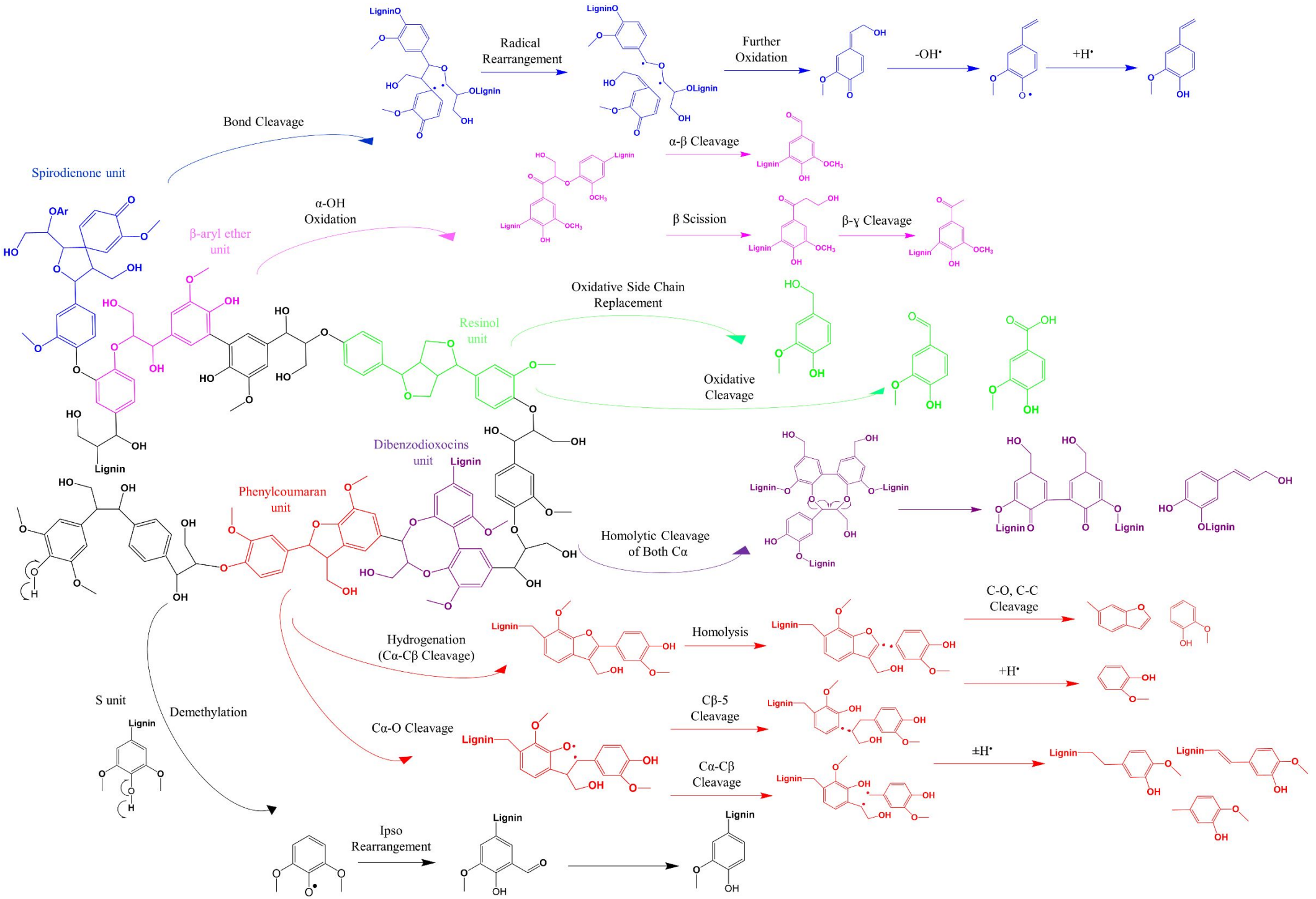

Figure 7: Possible lignin degradation pathway in oxidation systems and the generated monomers[37, 51, 61, 69, 71]

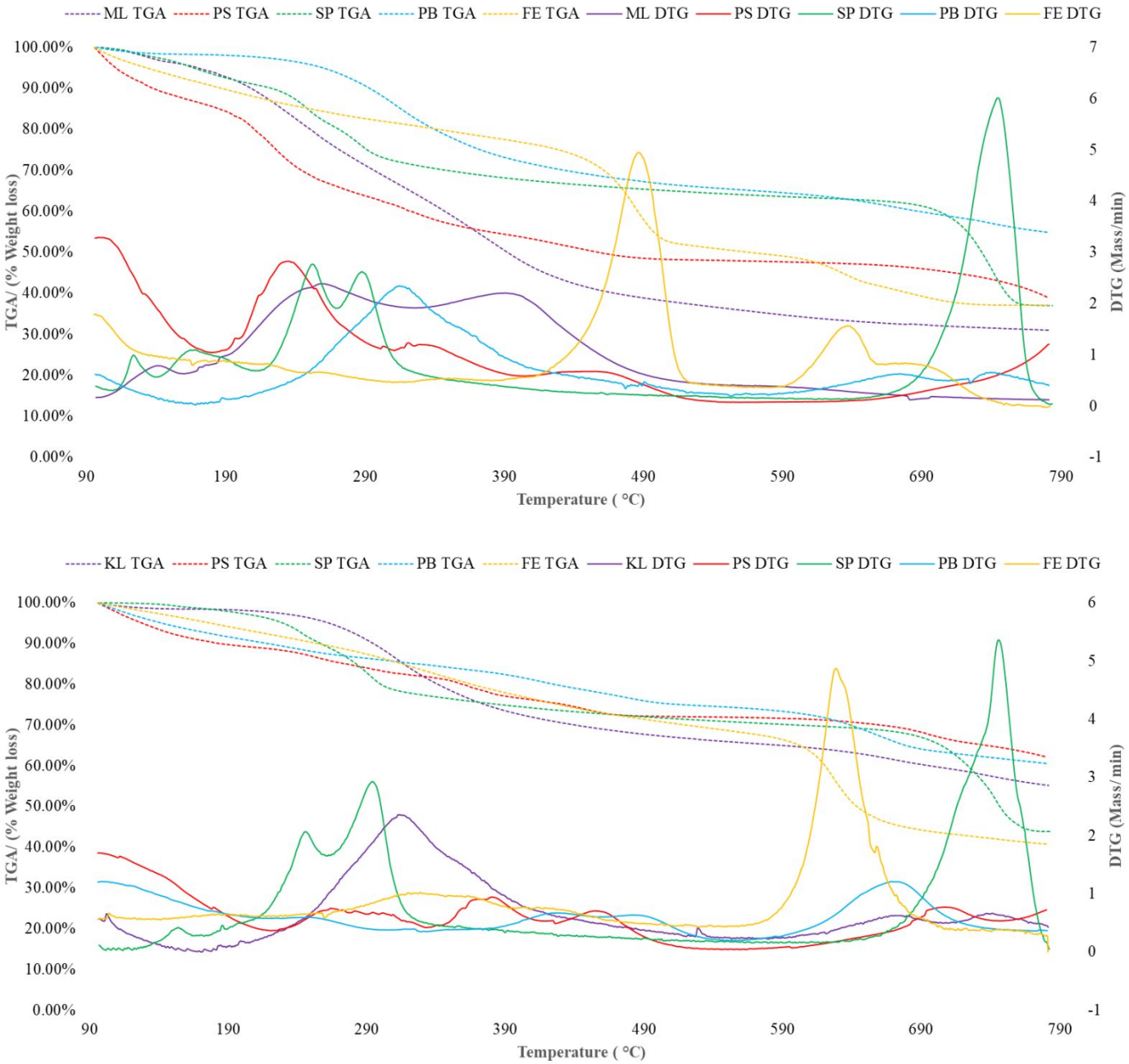

Figure 8: TGA and DTG for four Milled and Kraft lignins before and after oxidation (heating rate of 10 °C/min). Lignin structures degradation under a wide temperature range due to its side chains and a variety of functional groups.